ENSO AND IOD IMPACT ANALYSIS OF EXTREME CLIMATE CONDITION IN PAPUA, INDONESIA

Sri NURDIATI [1 *], ***Fahren BUKHARI*** [1], ***Ardhasena SOPAHELUWAKAN*** [2], ***Pandu SEPTIAWAN*** [1], ***Vicho HUTAPEA*** [1]

DOI: 10.21163/GT_2024.191.01

ABSTRACT:
Papua, known as one of the wettest regions in the world with annual precipitation ranging from 2400 to 4500 mm, faces a high risk of flooding, especially during La Niña, as observed in 2018 and 2022. Conversely, the region also experiences forest fires, mainly in the southern areas of Papua, during periods of extreme dry conditions brought about by El Niño events, as seen in 2002, 2004, and 2015. Given the increasing frequency of extreme climate events in the context of climate change, understanding the impact of global climate phenomena such as El Niño Southern Oscillation (ENSO) on Papua is crucial. This research aims to analyze the influence of ENSO and the Indian Ocean Dipole (IOD) on forest fires and flood risk in Papua, Indonesia. The analysis of forest fires utilizes MODIS hotspot and ERA5 precipitation data, employing quantitative modeling techniques such as Lasso and Elastic Net Regression. It integrates both ENSO and IOD indices into the precipitation indicators. In contrast, flood analysis is carried out through distribution and joint pattern analysis. The Elastic Net Regression yields promising results in modeling, with more than 96% of the tested models successfully predicting the total annual hotspots for each year, achieving an R-squared value of 90%. This suggests that the method and algorithm used can serve as a robust model for early hotspot prediction in the analyzed area. The warm phases of ENSO and IOD consistently exhibit a positive correlation with the dry season. However, the cold phases of these phenomena do not significantly impact heavy and extreme precipitation indicators in the studied region. The flood analysis reveals that La Niña has only a slight effect on all three precipitation patterns in the analyzed area, primarily by increasing the risk of extreme precipitation indicators. Conversely, negative IOD demonstrates inconsistency across all three precipitation patterns in Papua.

Key-words: *Climate, ENSO, IOD, Forest Fire, Flood Analysis, Indonesia*.

1. INTRODUCTION

As a maritime country placed between 2 oceans, Indonesia has a high variability of precipitation. Even more, when global phenomena such as El Niño Southern Oscillation (ENSO) and Indian Ocean Dipole (IOD) happened, especially from September to November (Hidayat et al., 2016, Hendon, 2003). *El Niño* The Southern Oscillation (ENSO) is a climate anomaly that occurs due to the interaction phenomenon between the atmosphere and the waters of the Pacific Ocean (Cane & Zebiak, 1985). The Indian Ocean Dipole (IOD) is a climate anomaly that occurs due to the phenomenon of interaction between the atmosphere and waters in the Indian Ocean, measured using DMI which is defined as the difference in sea surface temperature anomaly in the Western Tropical Indian Ocean (50°E-70°E/ 10°S – 10°N) and sea surface temperature anomaly in the Southeastern Tropical Indian Ocean (90°E- 110 °E / 10°S – 10°N) (Saji et al., 1999). The warm phase of both phenomena (El Niño for ENSO, +IOD for IOD) will decrease precipitation in Indonesia. Meanwhile, Indonesian precipitation increases during their cold phase (La Niña for ENSO, -IOD for IOD) (Pawitan, 1999; Iskandar, 2022).

[1]*IPB University, Department of Mathematics, 1680, Bogor, Indonesia. Corresponding Author nurdiati@apps.ipb.ac.id, fahrenbu@apps.ipb.ac.id, septiawan.pandu@gmail.com, vicho_hutapea29@apps.ipb.ac.id,*
[2]*Agency for Meteorology, Climatology and Geophysics, Center for Applied Climate Services, 10720, Jakarta, Indonesia, ardhasena@gmail.com*

Independently, both phenomena have proven to have correlation with Papua precipitation, especially ENSO. There is a notable strong positive connection between the Indian Ocean Dipole (IOD) and the rainfall in Indonesia over a time span of approximately 2.5 to 4 years. Additionally, a significant positive correlation between the El Niño-Southern Oscillation (ENSO), specifically the sea surface temperature anomaly in the Niño3.4 region, and Indonesian rainfall is observed on shorter time scales, lasting less than 2 years and between 5.5 to 6.5 years (Hendrawan et al., 2019). The influence of ENSO on the start and end of seasons in Indonesia is more visible in eastern regions such as Sulawesi, Maluku, and Papua than in western regions such as Java and Sumatra (Rahmawati, Idung & Fadli 2011).

Using multi-sensor remote sensing data, southern part of Papua is considered as ENSO sensitive region (Arjakusuma et al., 2018). During June – November, Papua has significant negative correlation with Nino3.4 (Okta et al., 2018). The decrease/increase of precipitation on each year is depended on the strength of the phenomena (Kurniadi et al., 2021; Sarvina, 2023). In the long period, the decreased precipitation will increase the risk of forest fire events triggered by many hotspots occurring in the dry season. The analysis conducted under the CIMP5 projection reveals that, in future conditions (2006-2035), ENSO is expected to be more intense than IOD, with ENSO reaching a very high intensity of up to 4°C expected to give drier condition in the future than historical events. Meanwhile, the increased precipitation will increase the risk of floods and landslides by increasing the frequency of heavy precipitation.

A hotspot serves as a commonly utilized indicator for the examination of forest fire occurrences, while precipitation and its anomalies are factors that influence the rate at which hotspots emerge (Syaufina et al., 2004; Ceccato et al., 2010). When El Niño and +IOD coincide, there is a substantial impact, with precipitation decreasing by up to 200 mm per month (Ngestu, 2016). This reduction in rainfall can result in drier land conditions that are more susceptible to ignition and, consequently, forest fires. According to Times Indonesia's report on August 7, 2017, Sutopo Purwo Nugroho, who served as the Head of the Center for Information Data and Public Relations of the National Disaster Management Agency (November 2010 - July 2019), noted that there were 158 forest and land fire hotspots in Indonesia on that day, with 93 of them located in Papua. The number of hotspots had risen significantly from just 7 the previous day (August 6, 2017). Since 2015, forest and land fires have been widespread in Papua. Therefore, it is imperative to develop a model that assesses the impact of ENSO and IOD on hotspot formation in Papua. This modeling can serve as a valuable tool for predicting hotspot occurrences in Papua and designing preventive measures to mitigate the adverse effects of hotspot incidents.

Papua, in the absence of ENSO and IOD phenomena, is one of the rainiest regions in the world, receiving annual rainfall ranging from 2400 to 4500 mm (Prentice & Hope, 2007). Geographically, Papua's rainfall pattern can be categorized into three distinct types: monsoonal, equatorial, and local. The local pattern is predominantly observed in West Papua province, while the other two patterns dominate in Papua province. The diverse geographical conditions, along with the coexistence of these three rainfall patterns, contribute to a wide range of precipitation patterns in Papua, making it a complex area for robust analysis, particularly in the context of floods and landslides.

The primary goal of this study is to model the impact of ENSO and IOD on forest fires and floods in Papua. However, due to the limited availability of flood data, the weight function analysis is exclusively applied to the forest fire phenomenon. This weight function is designed to enhance the correlation between the model data and hotspot data. Moreover, the weighting function is evaluated to understand the interplay between variables and to derive spatial and temporal patterns and plots. Simultaneously, the analysis of flood and landslide risk in this research is conducted by examining the characteristics of extreme precipitation indicators, including consecutive wet days, the number of days with heavy precipitation, the number of days with very heavy precipitation, very wet day precipitation, and extreme wet day precipitation in Papua. This analysis employs joint principal component analysis to link sea surface temperature with each extreme precipitation indicator utilized.

2. DATA AND METHODS

This research is structured into two main sections, each aligning with its respective objective. The first section is dedicated to examine and model the forest fires in Papua, while the second section focuses on investigating flood and extreme precipitation risks in the studied region. The fires risk will be modeled and analyzed using regression models based on Lasso and Elastic Net Regression (ENR). Meanwhile, the extreme precipitation risk analysis will be conducted through distribution and principal component analysis. The principal component analysis will be using combined singular value decomposition concept to analyses joint pattern between extreme precipitation, ENSO and IOD SST. The research steps follow the sequence outlined in **Fig. 1**.

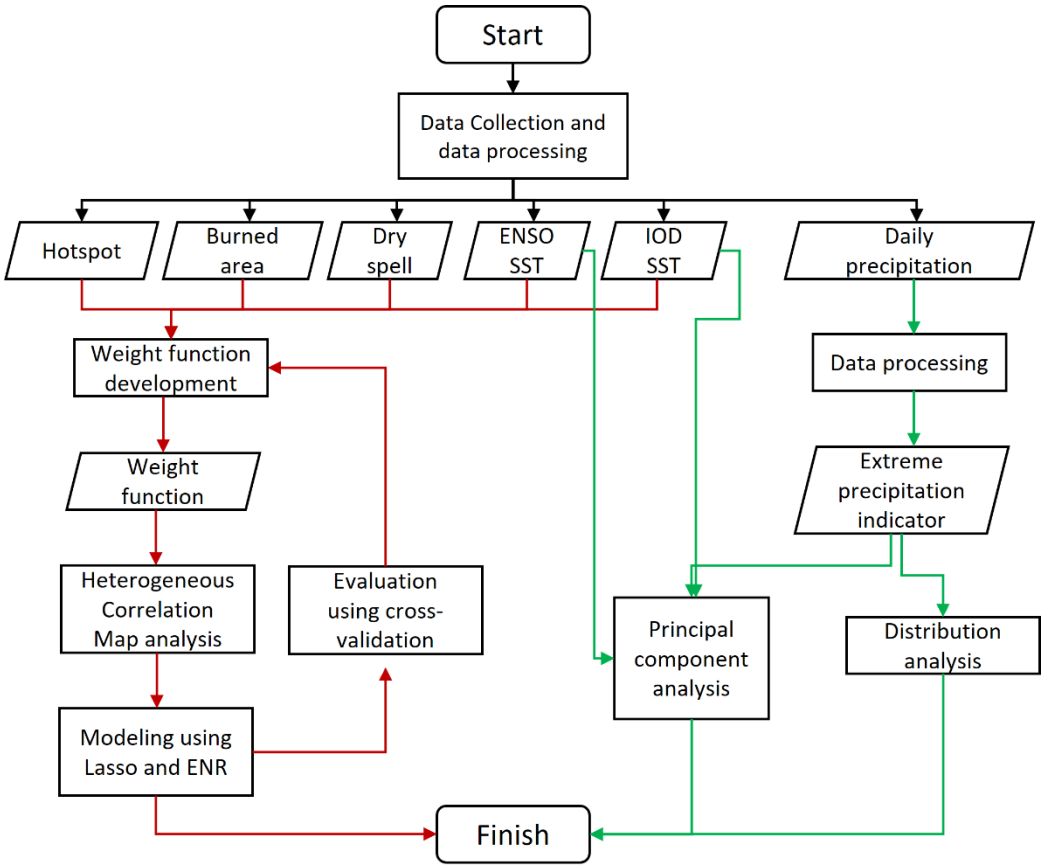

Fig. 1. Research Flow.

2.1. Climate data

This research begins by conducting a literature study related to the data and methods used. The first data used is daily hotspot data in the Papua region sourced from NASA's Moderate Resolution Imaging Spectroradiometer (MODIS). This data can be freely accessed and downloaded via the website: https://earthdata.nasa.gov/ (Schroeder et al., 2014). The hotspot data is processed so it has a grid resolution of 0.10° × 0.10° and cover daily data from 1 June 2001 to 31 May 2021. In order to add more information about forest fire in Papua, we add burned area data obtained from Global Fire Emissions Database (GFED) from 2001-2015 (Randerson et al., 2018). The next data is Reanalysis 5-th Generation (ERA5) hourly data on single levels by taking total precipitation variable. The data

can be accessed via the page: https://cds.climate.copernicus.eu/cdsapp#!/dataset/reanalysis era5-single-levels?tab=form. The data is produced by the European Center for Medium-Range Weather Forecast (ECMWF) (Hersbach et al., 2020). Despite of the availability of the ERA5 data, it is chosen because of the process that carried when building ERA5 data. ERA5 data is modeled data that corrected and reanalyzed using observation data, thus it has good accuracy while maintaining the general predictability of the data. The data is hourly data for June 2001 – May 2021 and has a grid resolution of 0.10° × 0.10° in meters (m). Other climate relate data will be derived from this precipitation data.

Dry spell data is monthly that obtained by counting the number of days that have less than 1 mm in a month. Consecutive Wet Days are monthly data that measure the maximum number of days that have precipitation more than 1 mm. The number of Heavy Precipitation Days is obtained by counting the number of days when precipitation more than 10 mm. The number of very heavy precipitation days is derived from days when precipitation is more than 30 mm. Very wet days precipitation is obtained by calculating daily precipitation that is over its 95th percentile, while extreme wet days precipitation is derived from the 99th percentile one. The last data is related to ENSO and IOD's SST which was obtained from HadiSST (Rayner et al., 2003). The used index is derived from these datasets. The method used for the evaluation process is HCM analysis. In this study, data processing was carried out using MATLAB R2021a software.

2.2. Forest Fire Risk Calculation

The forest fire analysis will be done by modeling dry spell data (weighted using global climate indices) to monthly hotspot data. The use of weight function is followed by previous research (Nurdiati et al., 2021; Ardiyani et al., 2023). Denote the weight function as a polynomial equation:

$$w\left(ENSO_{log}, IOD_{log}; a, b, c, d\right) = a.ENSO_{log} + b.IOD_{log} + c.ENSO_{log}.IOD_{log} + d, \quad (1)$$

$$ENSO_{log}(t; \theta_1, \theta_2, \theta_3) = {\theta_1}\Big/{1 + \exp\left(-\theta_2.\left(ENSO(t) - \theta_3\right)\right)}, \quad (2)$$

$$IOD_{log}(t; \theta_4, \theta_5, \theta_6) = {\theta_4}\Big/{1 + \exp\left(-\theta_5.\left(IOD(t) - \theta_6\right)\right)}, \quad (3)$$

with $a, b, c, d \in \mathbb{R}^+$represent the independent impact of ENSO, independent impact of IOD, joint impact of ENSO and IOD, and other factors that influence forest fire in Papua respectively.

The value of each coefficient is obtained unrestricted optimization process with the objective function of maximizing the Chatterjee correlation between hotspot and weighted dry spell.

The Chatterjee correlation was recently developed by Sourav Chatterjee (2021) which is a function of ranks. Thus, makes it robust to outliers and invariance under monotone transformations of the data. Despite that, due to its simple formula, it is easy to understand conceptually and computable very quickly, not only in theory but also in practice. It has a very simple asymptotic theory under the hypothesis of independence, which is roughly valid even for samples of size as small as 20. The coefficient correlation is defined as:

$$\xi_n(X_i, Y_i) \coloneqq 1 - \left(3\sum_{i=1}^{n}|r_{i+1} - r_i|\right)/(n^2 - 1), \quad (4)$$

where X_i and Y_i are the variables, and Y is not a constant. i represents the index from 1 to $n - 1$, and r_i represents the rank of $Y_{(i)}$. Using this coefficient correlation, the optimization follows Eq. below:

$$\arg\max_{a,b,c,d} \xi_n(Ds_i.w(ENSO, IOD; a, b, c, d), Y_i). \quad (5)$$

The advantages of the weighted function are assessed both in terms of spatial and temporal aspects. Spatial analysis is conducted using Heterogeneous Correlation Maps (HCM), while temporal analysis is demonstrated through the utilization of Lasso regression and Elastic Net Regression (ENR). Lasso regression is chosen for its excellent performance and efficiency, making it a recommended tool for detecting teleconnections and understanding physical mechanisms in the Earth's climate system (Li, Pollinger & Paeth, 2020). On the other hand, ENR is employed to address the limitations of Lasso regression when dealing with a high number of variables (Al Jawarneh, Ismail & Awajan, 2021).

The HCM analysis in this research is based on the outcomes of coupled Singular Value Decomposition (SVD) (Bjornsson & Venegas, 1997) using dry spell and hotspot data. The evaluation process involves calculating the correlation coefficient for each grid location of both raw data and weighted data. The process is followed in Eq. below, with Hs representing the hotspot matrix while Ds represent dry spell data.

$$X = HsDs^T, \tag{6}$$

$$X = U\sum V, \tag{7}$$

$$E_1 = U^T Hs, \tag{8}$$

$$E_2 = V^T Ds. \tag{9}$$

U and V are singular vector of hotspots and dry spell matrices respectively (Navarra & Simoncini 2010).

Meanwhile, E_1 and E_2 are expansion coefficients of hotspots and dryspell, respectively. The HCM of hotspot is provided by calculating the correlation between E_2 and Hs.

Lasso (least absolute shrinkage and selection operator) regression is a linear regression-based method that minimizes the residual sum of squares subject to the sum of the absolute value of the coefficients being less than a constant (Tibshirani, 1996). as variable selection becomes increasingly important in modern data analysis, the lasso is much more appealing owing to its sparse representation. Defined *X* as predictor, and *y* as responses variable. With the assumption of either observations are independent or that *y* is conditionally independent given the *X* as well as *X* are standardized, the lasso estimate ($\hat{\beta}$) is defined by

$$\hat{\beta}_{lasso} = \arg\min_{\beta} \beta^T (X^T X)\beta - 2y^T X\beta + \lambda_1 |\beta|_1. \tag{10}$$

However, since we use climate data that will not be completely independent and Lasso regression is not a very satisfactory variable selection method if the number of predictors is much bigger than the number of observations. Therefore, we use ENR to give supporting results when Lasso regression does not perform as great as expected. ENR is a hybrid of ridge regression and lasso regularization. Like lasso, the elastic net can generate reduced models by generating zero-valued coefficients but is often more powerful when predictors are highly correlated (Zou & Hastie, 2005). Given data (*y*,*X*), and (λ_1, λ_2), the elastic net estimates $\hat{\beta}$ are given by

$$\hat{\beta}_{ENR} = \arg\min_{\beta} \beta^T \left(\frac{X^T X + \lambda_2 I}{1+\lambda_2}\right)\beta - 2y^T X\beta + \lambda_1 |\beta|_1. \tag{11}$$

The performance of the regression will be shown using cross-validation analysis using 17 years of combination as training data and 3 years as testing data.

2.3. Flood Risk Calculation

The flood and landslide analysis in this research is unable to be done using a similar analysis to the forest fire one. This is caused by the lack of availability of satellite-derived data that can be used to measure flood and landslide well in large-scale domains. Therefore, the analysis is provided by distribution analysis and measuring the joint pattern between extremely high precipitation indicators (Consecutive Wet Days, Number of Heavy Precipitation Days, Number of Very Heavy Precipitation Days) with Sea Surface Temperature (SST) related to ENSO and IOD phenomena. The first three indicators are fitted with Gamma distribution (Choi & Wette, 1969), while two others are fitted with Generalized Extreme Value distribution (Haan & Ferreira, 2007) following the probability density function below, respectively:

$$f(x;\alpha,\beta) = (x^{\alpha-1}e^{-\beta x}\beta^{\alpha})/\Gamma(\alpha) \text{ for } x > 0, \alpha, \beta > 0, \Gamma(\alpha) \text{ is the gamma function} \quad (12)$$

$$f(x;\sigma,\xi) = \sigma^{-1}t(x)^{\xi+1}e^{-t(x)}, \text{ where } t(x) = \begin{cases} (1+\xi\left(\frac{x-\mu}{\sigma}\right)^{-1/\xi} & if\ \xi \neq 0 \\ e^{-(x-\mu)/\sigma} & if\ \xi = 0 \end{cases}. \quad (13)$$

$\mu \in \mathbb{R}$ is location parameter, $\sigma > 0$ is scale parameter, $\xi \in \mathbb{R}$ is shape parameter of the generalized extreme value distribution.

The joint pattern of individual impact from both phenomena is obtained using coupled SVD (Eq. 4-7). Meanwhile, the joint impact of both phenomena is examined using combined SVD (Navarrra & Simonchini, 2010) follow Eq. bellow.

$$Z = \begin{pmatrix} Extreme\ Precipitation\ Indicators \\ ENSO's\ Sea\ Surface\ Temperature \\ IOD's\ Sea\ Surface\ Temperature \end{pmatrix}, \quad (14)$$

$$Z = U\sum V, \quad (15)$$

U is singular vector that is used to analyzed the spatial characteristic of each indicator, while V is used to analyzed the temporal characteristic of joined phenomena.

SVD used as its powerful ability to extract independent pattern from complex data (Hannachi, Jolliffe & Stephenson 2007; Hui et al., 2021). In order to make the temporal pattern easier to analyzed, the patterns are transformed using Fourier transformation defined as

$$F(v) = \int_{-\infty}^{\infty} f(x)e^{-i2\pi vx}dx, \quad (16)$$

with $e^{-i2\pi vx}$ called kernel function, $f(x)$ is time series vector, $F(v)$ is vector with frequency domain (Wiley, 2014).

Using Fourier transformation, the temporal patterns are converted from time series vector in to vector with frequency domain. Therefore, we will be able to determined period of each joint pattern. The computational aspect is done using Fast Fourier Transformation concept introduced by Brenner & Rader (1976).

3. RESULTS

3.1. Forest Fire Analysis

For the last 20 years, Papua has suffered for multiple annual forest fires. Using the MODIS active fire count data, the average of monthly hotspot occurred in Papua is 6.2 with each data point in range value of 3 to 90 hotspot. During the period, there are 91 extreme events with more than 13 hotspots occurred in a single month for each analyzed grid (**Fig. 2**). Meanwhile, the GFED data shows that there are 1051 extreme events occurred in the 2001-2015 data in 95th percentile with more than 2 ha area burned on 0.25° × 0.25°grid data during the period.

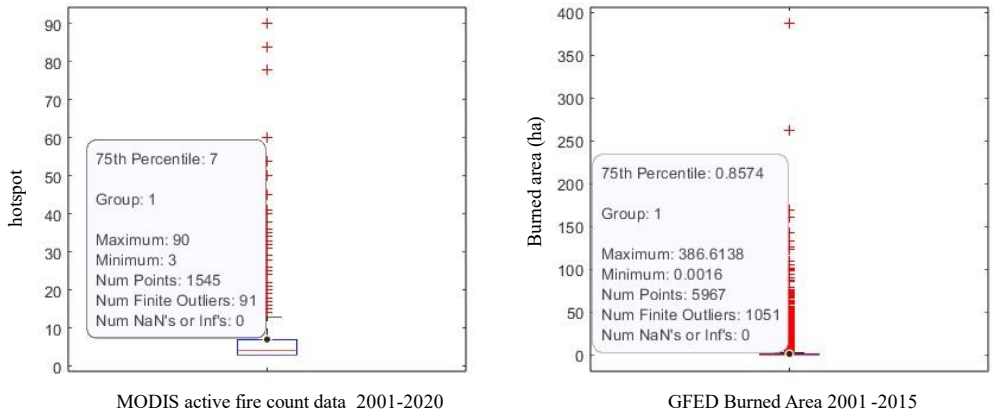

Fig. 2. Hotspot and Burned area characteristic in Papua.

In the forest fire analysis, the dry spell data is generated as a weighted function, as defined in Eq. 1. This function incorporates transformed ENSO and IOD indices, following the formulas given in Eq. 2-3. The dry spell data itself represents the accumulation of the three most recent months of the event, spanning from June 2001 to May 2021. The coefficients for Eq. 1-3 are determined through an unconstrained optimization process. This process aims to maximize the correlation between hotspots and the weighted dry spells. To ensure that the ENSO and IOD indices align with the desired range, a logistic transformation is applied. This transformation scales both indices to have a minimum value of 0, indicating no influence on the dry season, and a maximum value corresponding to each index's original range, while following the shape of a general logistic curve.

The initial values for this transformation process are randomized, and this is done using 10,000 different seeds in Matlab. The best coefficient is obtained using maximum Pearson linear correlation, resulting in function:

$$w(ENSO_{log}, IOD_{log}) = 1.217ENSO_{log} + 1.558IOD_{log} + 0.707ENSO_{log}.IOD_{log} + 1.738, \quad (17)$$

$$ENSO_{log}(t) = {}^{0.718}/_{1 + \exp(-1.991(ENSO(t) - 1.374))}, \quad (18)$$

$$IOD_{log}(t) = {}^{1.446}/_{1 + \exp(-3(IOD(t) - 1.529))}. \quad (19)$$

Based on the coefficients in Eq. 17, it is evident that most hotspots are not significantly associated with both the ENSO and IOD indices. In contrast, individual ENSO and IOD indices show slight differences in their influence, with the combined impact of both phenomena being the least influential. Although there are only modest enhancements in spatial correlation, Eq. 17-19 successfully raise the temporal Pearson linear correlation value between the total hotspot and the dry spell data from 0.5523

(raw data) to 0.8644 (weighted data) (**Fig. 3**). As a result, the predictability of monthly hotspots in Merauke has considerably improved in the regression analysis. In this research, regression modeling is carried out using the total dry spells in the last 3 months and the precipitation in the last month as predictors for each grid. The total monthly hotspots in the entire observed area serve as the response variable. Due to limited data, the evaluation of the modeling is conducted using the cross-validation approach. Three years of data are reserved for testing, while the remaining data is used to train the model. A summary of the results is presented in **Fig. 4** for both Lasso regression and Elastic Net Regression (ENR).

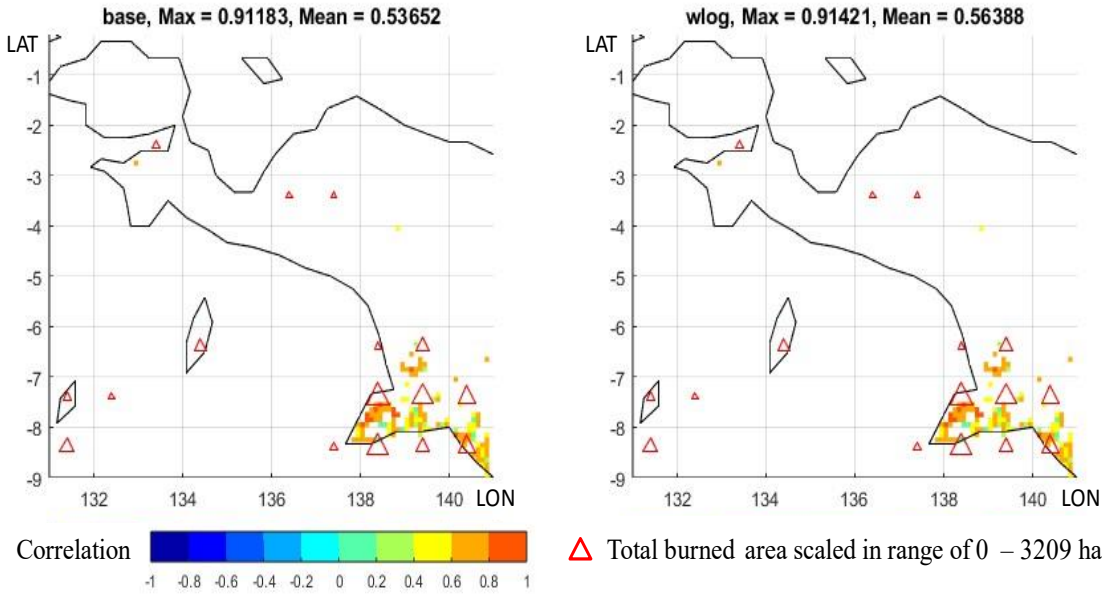

Fig. 3. Heterogeneous correlation maps between dry spell – hotspot and weighted dryspell – hotspot.

Fig. 4 illustrates that the use of weighted dry spell data significantly enhances the modeling of raw data when applied to each year, with the exception of 2015 when using Lasso regression. In the case of models predicting hotspot values in 2015, only 23% of the weighted models achieve an R^2 value exceeding 90%, while raw data can yield this level of accuracy in 34% of models. Among models using Lasso regression, the most challenging years to predict are 2001, 2009, and 2019, while the easiest are 2002, 2004, and 2018. On average, only around 37% of models achieve an R^2 exceeding 90%. This result suggests a high degree of correlation among predictors, and the elimination of predictors using Lasso regression principles can lead to diminished regression performance. It also highlights that Lasso regression underperforms when the number of predictors (1171) exceeds the number of observations (120). It is worth noting that the regression is exclusively conducted during monsoonal dry season months in the analyzed area, which span from June to November.

The advantage of using weighted dry spells becomes particularly pronounced when performing cross-validation in Elastic Net Regression (ENR). ENR, on its own, enhances the performance of raw data regression, with approximately 66% of models achieving an R^2 value exceeding 90%. However, the weighted function defined in Eq. 17-19 significantly boosts the regression performance, with more than 96% of models achieving an R^2 value exceeding 90%. Although further testing is necessary with different analyses, this method has the potential to become a robust early algorithm for predicting hotspots in the analyzed area, regardless of the conditions related to ENSO and IOD phenomena. A few comparison examples of the obtained models are presented in **Fig. 5**.

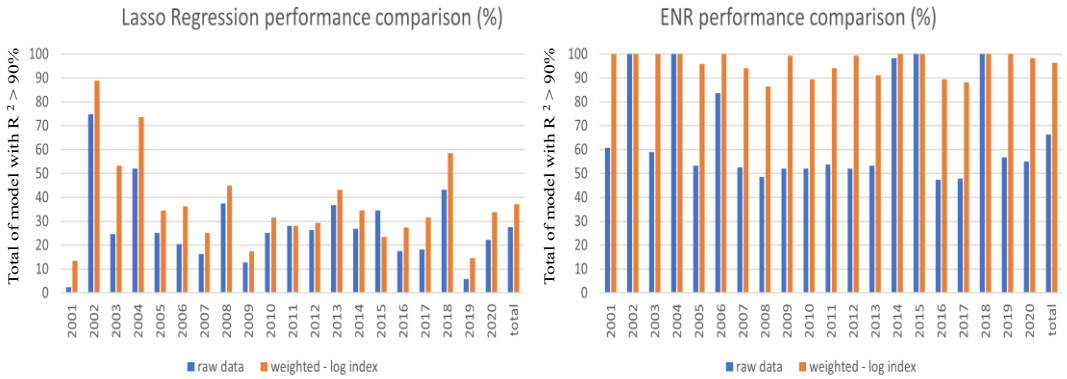

Fig. 4. Total number of models in lasso regression and ENR that have R^2 value more than 90%.

Based on the model examples shown in **Fig. 5**, the weighted models tend to produce lower predicted hotspot values than the raw models. This suggests better performance when predicting small-scale fire events. Considering that most fire events in the analyzed area are small, typically ranging from 200 to 800 hotspots during peak fire events, the weighted models are more robust, as demonstrated in **Fig. 4**. However, the use of weighted models may have limitations when estimating large-scale fire events, such as those observed in 2002 and especially in 2015, which had significantly more hotspots than other years, as indicated by the error graph in **Fig. 6**.

The performance of weighted models when used to predict the year 2002 varies depending on the data used to train the models. When used to predict 2002, 2004, and 2018, weighted models outperform raw models for 2002 with a significantly lower error. However, when used to predict 2002, 2004, and 2009, the performance decreases substantially. This reduction is due to the absence of El Niño years in the training data, as all three tested years are El Niño years. A similar trend is observed when predicting 2006, 2015, and 2019, which are years with a positive Indian Ocean Dipole (+IOD). The removal of these years from the training data leads to a significant decrease in model performance. This is expected because the weighted models directly incorporate the impacts of both ENSO and IOD into the models, making the presence of years with ENSO and IOD crucial for performance.

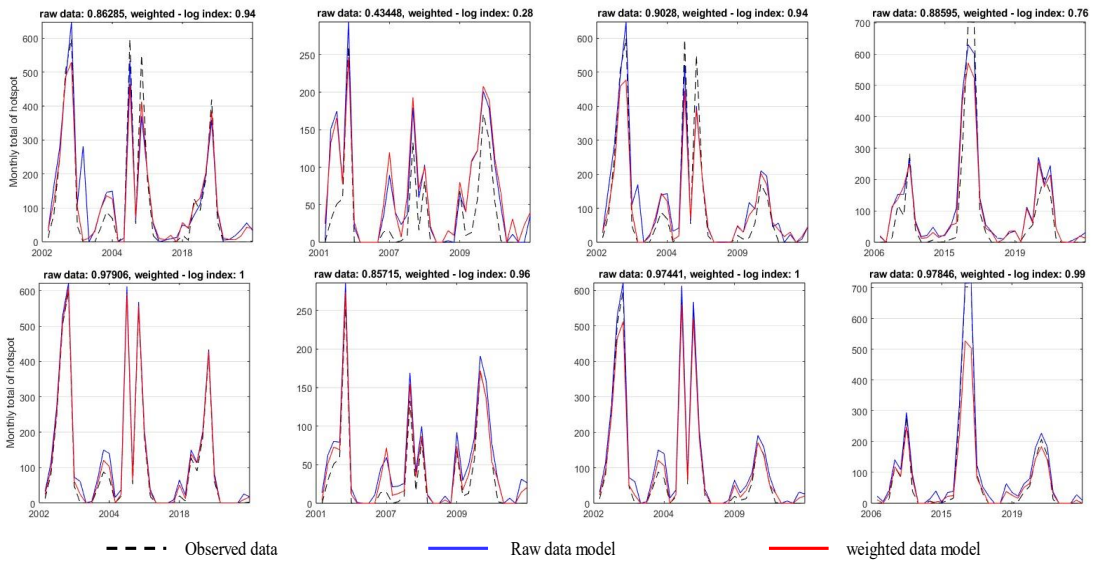

Fig. 5. Model performance when used to predict certain years: top: Lasso regression, bottom: ENR.

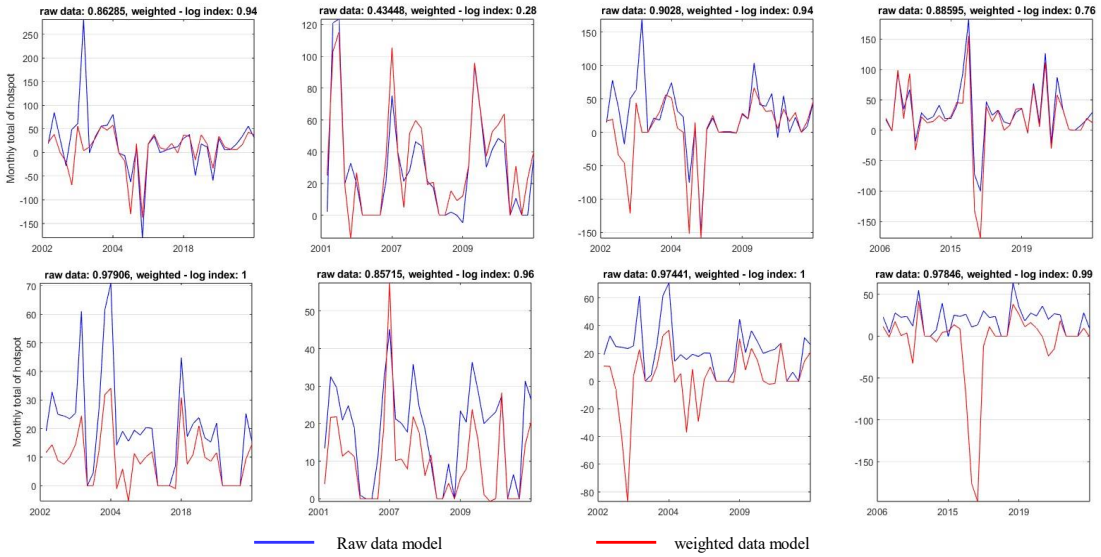

Fig. 6. Model error when used to predict certain years: top: Lasso regression, bottom: ENR.

3.2. Flood Risk Analysis

As mentioned before, the flood analysis is done using an entirely different approach than that of forest fire analysis. This is done due to the lack of availability data on floods in observed areas. The analysis is conducted through five precipitations-based indicators, namely:

- consecutive wet days: Maximum number of consecutive days with daily precipitation ≥ 1 mm,
- number of heavy precipitations: Monthly count of days with daily precipitation ≥ 10 mm,
- number of very heavy precipitations: Monthly count of days with daily precipitation ≥ 30 mm,
- very wet day precipitation: Monthly total precipitation when daily precipitation > 95th percentile,
- extreme wet day precipitation: Monthly total precipitation when daily precipitation > 99th percentile.

All of the analyzed indicators are obtained using daily ERA5 precipitation data with spatial observation is 0.1˚×0.1˚. The monthly data is processed to include accumulated climate information for the past three months. The first characteristic of each variable is assessed by analyzing their probability density function curves, with data being divided based on the average values of Niño3.4 or DMI for the preceding three months. A threshold of 0.5 is used to distinguish El Niño, and -0.5 indicates La Niña for ENSO. For IOD, a threshold of 0.4 is used for +IOD, and -0.4 for -IOD, relative to normal years. This data separation is carried out on a monthly basis rather than a yearly basis to ensure more precise results. Consequently, this approach provides a comprehensive understanding of the influence of ENSO and IOD on extreme wet precipitation indices in the analyzed area.

Utilizing the gamma distribution for the first three variables and the generalized extreme value distribution for the others, it's evident that El Niño has a minimal impact on the distributions of all the analyzed variables, as shown in **Fig. 7**. In contrast, La Niña exerts a noteworthy influence, especially on the distribution of the number of days with heavy precipitation in the last 3 months. This behavior aligns with expectations since La Niña tends to correlate positively with increased precipitation in Indonesia. However, the surprising finding is the impact of El Niño, where the risk of flooding does not decrease during El Niño. This result suggests that the analyzed area has a consistently high risk of flooding regardless of the ENSO condition. Distinct patterns emerge when the data is separated using the Dipole Mode Index (DMI). Both +IOD and -IOD significantly affect the risk of extreme precipitation compared to normal years. While the influence of a -IOD is anticipated, the impact of a +IOD warrants further investigation through additional analyses.

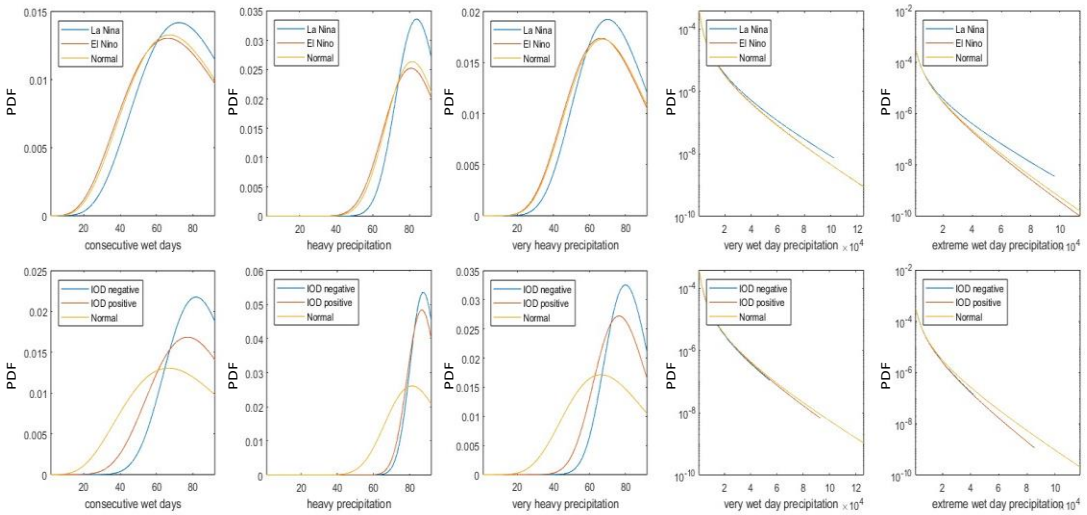

Fig. 7. PDF comparison for each analyzed variable in different ENSO/IOD condition.

This pattern is consistent with the results observed for very wet days' precipitation and extreme wet days' precipitation. IOD seems to have minimal effects on the distribution of very wet days' precipitation in normal years but shows lower values for extreme wet days' precipitation. In conclusion, the analysis suggests that IOD does not consistently influence extreme precipitation in the analyzed area.

Fig. 8 presents the comprehensive outcomes of the combined Singular Value Decomposition (SVD) between consecutive wet days, Niño3.4 Sea Surface Temperature (SST), West IOD SST, and East IOD SST. The combined data is standardized to have a mean of 0 and a standard deviation of 1 for each column (time dimension) to remove data domination since the extreme precipitation indicators have a wider data range compared to others. The spatial values are directly represented using the joint spatial pattern, where positive values indicate a higher occurrence of heavy precipitation in the pattern. The temporal pattern is displayed after transformation using Fourier transformation, which allows for a clearer understanding of the period of joint patterns present in the data, especially when dealing with the four combined variables.

When examining the temporal patterns, it becomes apparent that the joint patterns are divided based on the precipitation type within the analyzed area. The first joint pattern corresponds to heavy precipitation occurring in regions characterized by equatorial and monsoonal precipitation types. Equatorial precipitation affects the near-equator region of Indonesia and exhibits a seasonal period of 6 months. In contrast, monsoonal precipitation is influenced by monsoon winds and has a seasonal period of 12 months. Both precipitation types contribute to heavy precipitation in the analyzed area within the 1st mode spatial pattern, which has a value greater than 0. The 2nd joint pattern impacts the area opposite to that influenced by the 1st pattern, specifically the southern part of West Papua. This pattern exclusively influences regions with a monsoonal precipitation pattern, as evidenced by the 12-month period of the 2nd temporal pattern.

The 3rd joint pattern of consecutive wet days shares similarities with the 1st joint pattern in terms of seasonal periods (6 and 12 months), but it does not affect the analyzed area characterized by a local precipitation pattern. The local precipitation pattern is influenced by local climate and geography, resulting in contrasting precipitation conditions compared to monsoonal precipitation. This pattern is reflected in the 4th joint pattern. The differences in these patterns are a consequence of varying conditions in West IOD SST, East IOD SST, and Niño3.4 region SST. Across all joint patterns, the Niño3.4 SST region is predominantly characterized by negative values, indicating La Niña conditions. While not as clear and significant, West IOD SST consistently tends to have a higher average than East IOD SST, implying a -IOD phenomenon that is known to increase precipitation in Indonesia.

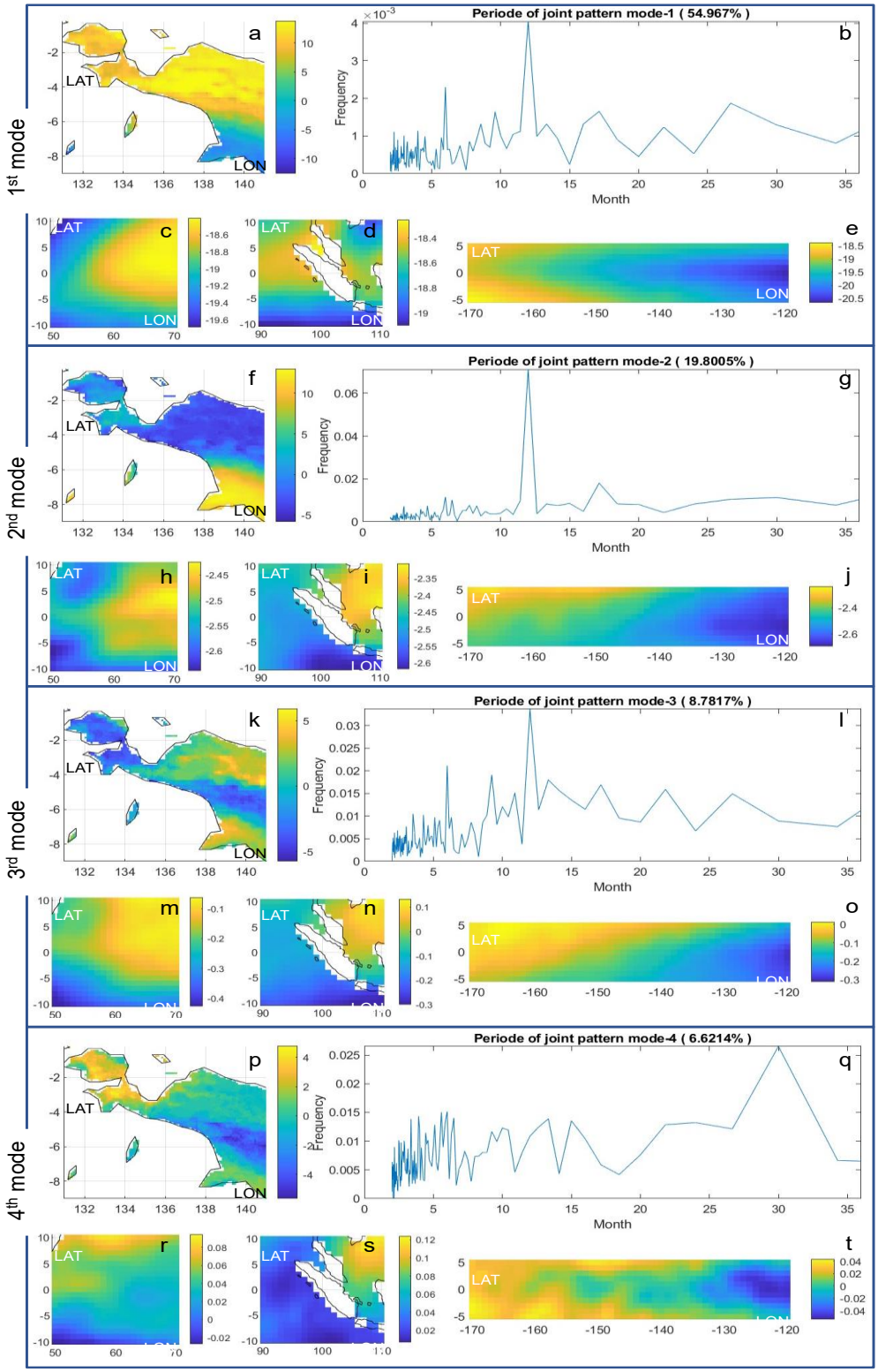

Fig. 8. Combined SVD result between standardized consecutive wet days, Niño3.4 Sea Surface Temperature (SST), west IOD SST, and east IOD SST.

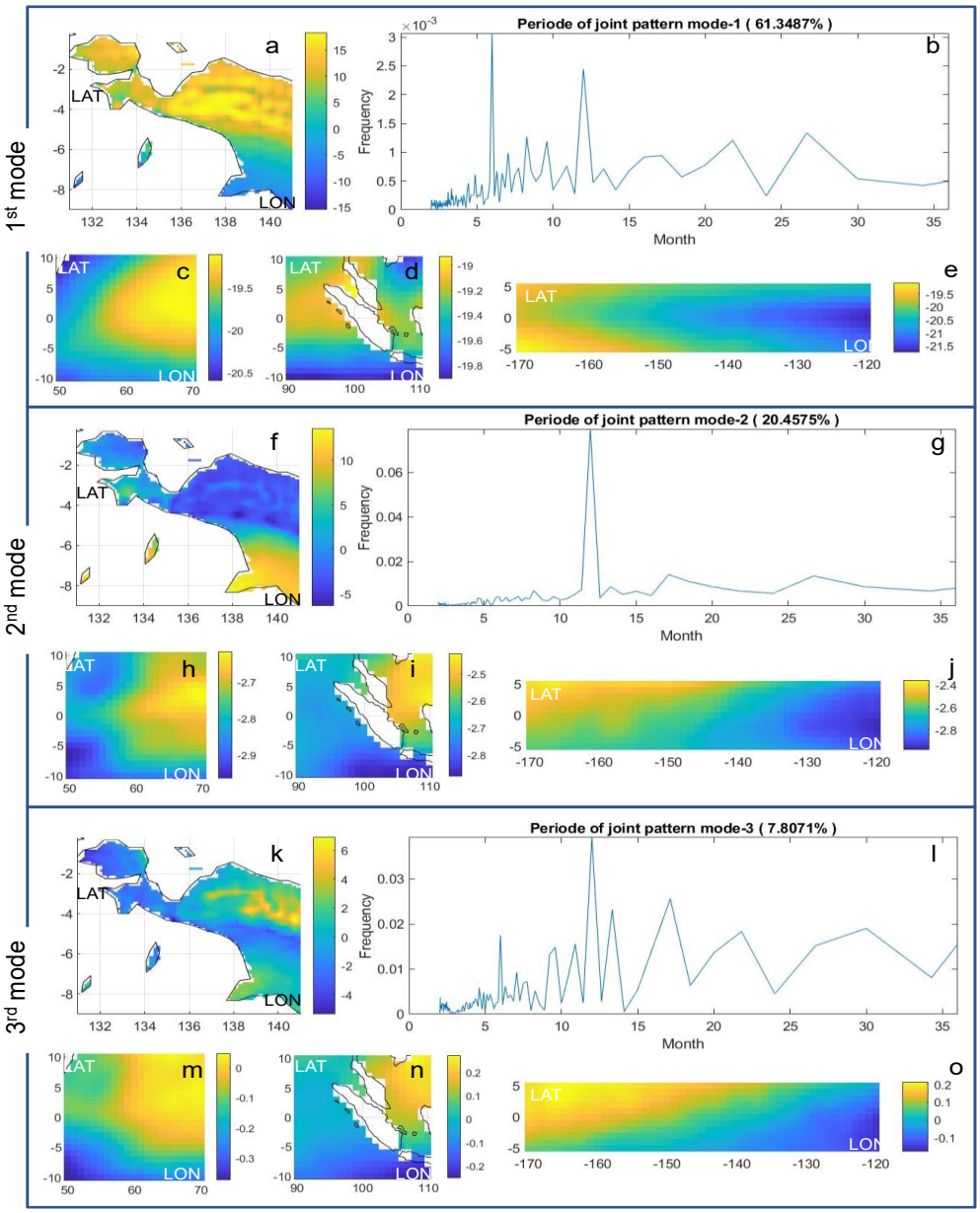

Fig. 9. Combined SVD result between standardized number of very heavy precipitation, Niño3.4 Sea Surface Temperature (SST), west IOD SST, and east IOD SST.

For consecutive wet days, four modes are required to explain around 90% of the variance. However, both heavy precipitation and very heavy precipitation only necessitate three modes (as seen in **Fig. 9**). As these two indicators yield nearly identical joint patterns, the focus here is on the joint patterns from very heavy precipitation analysis, which exhibits clearer distinctions between affected areas. The 2nd joint pattern is analogous to the analysis of consecutive wet days. However, the 1st and 3rd dominant patterns from very heavy precipitation differ primarily in the temporal perspective. The temporal pattern of the 1st joint pattern indicates that the first dominant pattern predominantly affects the equatorial region with an equatorial precipitation pattern. The temporal pattern also exhibits a higher frequency of 6 months compared to 12 months, indicating that the first extreme precipitation pattern occurs during La Niña when the monsoonal region is in the dry season.

On the other hand, the period when both precipitations are in the wet season phase is illustrated by the 3rd joint pattern, featuring high-frequency periods of 6, 12, and 18 months. In the analysis of heavy precipitation and very heavy precipitation, joint patterns affecting areas with local precipitation patterns tend to disappear. Depending on the research objectives, this may lead to incomplete results. Unfortunately, both very heavy and extreme wet days' precipitations do not yield distinct joint patterns that can be analyzed clearly; hence these results are not presented in the analysis.

4. DISCUSSION

4.1. Drought and Forest Fire Risk

ENSO and IOD are both well-established climate phenomena that influence precipitation patterns in Papua, especially during the June-July-October (JJA) and September-October-November (SON) seasons (Kurniadi et al., 2021). These phenomena, both individually and in combination, have been found to have positive correlations with decreased precipitation during El Niño and +IOD events, as well as increased precipitation during La Niña and -IOD events (Kurniadi et al., 2021). However, their impact during the December-January-February (DJF) and March-April-May (MAM) seasons remains less clear (Kurniadi et al., 2021). To minimize bias introduced by hotspots occurring during the wet season and being correlated with both ENSO and IOD, the forest fire models in this research focus on the period from June to November.

The results of the forest fire modeling, using hotspots as fire indicators, confirm previous research by providing positive coefficients in the weight function that contribute to both spatial and temporal aspects. Notably, the weight function's coefficient (Eq. 17) reveals that forest fires in Papua, Indonesia is influenced by events beyond ENSO and IOD (represented by the constant coefficient), which are not explained in the analysis. The contributions of both ENSO and IOD are significant, especially when both phenomena occur simultaneously. However, the independent impact of ENSO/IOD is not higher than the obtained constant coefficient in the Eq. 17. This result aligns with previous research that showed a significant decrease in impact when ENSO/IOD is calculated independently (Kurniadi et al., 2021). The positive coefficient indicates that ENSO and IOD have a positive correlation with drought conditions, which, in turn, result in forest fire events in Papua, Indonesia. This positive correlation suggests that El Niño and +IOD events tend to decrease precipitation in the analyzed area, while La Niña and -IOD events are associated with increased precipitation in the analyzed area. In the spatial analysis using the Heterogeneous Correlation Map (HCM), the incorporation of the ENSO-IOD weight function did not significantly improve correlation due to the high spatial correlation of raw data. Overall, this positive correlation confirms findings from previous composite analyses (Okta et al., 2018; Lee, 2015).

The advantage of integration is evident in the temporal analysis through Lasso and Elastic Net regression, with the latter performing significantly better. Lasso struggles when dealing with a high number of variables compared to the number of observations. Moreover, the underperformance of Lasso indicates that forest fires in the observed grid are not solely the result of climate conditions in that specific region but are also influenced by the surrounding climate. While it is essential to reduce the number of significant variables to minimize bias in modeling, Lasso regression's removal of contributions from less important variables leads to a substantial decrease in model performance. In this context, the Elastic Net Regression (ENR) principle, which reduces the significance of less important variables and eliminates unimportant variable contributions, is better suited to represent the relationship between climate conditions and forest fires in the analyzed area. The performance improvement achieved through the integration of the ENSO index emphasizes that the high occurrence of fire counts in the analyzed area is primarily influenced by both ENSO and IOD.

The performance gain is in line with previous research by Nikonovas et al. (2022), which achieved an accuracy of over 60% when focusing on areas primarily influenced by El Niño, including Papua, Indonesia. However, the limitation of the Nikonovas et al. (2022) model is its reduced performance in predicting areas influenced more by IOD or in years heavily affected by +IOD. This limitation can be mitigated by integrating IOD into the climate data, as done in this research using

Eq. 17 to improve predictability during IOD years, such as 2006 and 2019 **(Fig. 4)**. As a time-series prediction model, the results of this research could serve as robust predictive models for estimating total monthly hotspot occurrences using climate information from the past three months. However, further research is needed to accommodate probabilistic predictions, smaller time scales, and spatial information for more accurate anticipations. Integrating both ENSO and IOD into a single model is a priority, given the increased frequency of combined El Niño and +IOD events since the 1960s (Xiao, Lo & Yu, 2022).

4.2. Heavy Precipitation and Flood Risk

Flood risk analysis has been previously conducted using precipitation-based indicators, especially when observed data is challenging to obtain (Guerrerio & Lajinha, 2007; Breinl et al., 2021). In this context, the patterns and trends derived from such analysis are of great value to decision-makers for efficient flood risk management and the development of preventive strategies to mitigate the impacts of floods (Olanrewaju & Reddy, 2022). The Papua region is known for its highly diverse heavy precipitation patterns throughout the year. For instance, Jayapura exhibits unique rainfall with consistent precipitation values year-round. It experiences a 17% increase in annual precipitation during La Niña and approximately a 13% decrease in precipitation during El Niño (Sarvina, 2023). Meanwhile, Merauke's annual precipitation differs by less than 4% during El Niño and La Niña, and Manokwari experiences a noticeable difference primarily during La Niña (around 13%) (Sarvina, 2023).

At first glance, El Niño appears to have a limited influence on the high precipitation levels in Papua, Indonesia, as corroborated by the findings in this research (**Fig. 7**). While El Niño affects low precipitation levels during the dry season, it does not have a significant impact on the higher precipitation associated with flood risk. Its influence is only slightly observed in consecutive wet days, the number of heavy precipitation events, and extreme wet days. Notably, there are no noticeable differences between normal conditions and El Niño in the number of very heavy precipitations and very wet day precipitation. These results indicate that during the wet season, which carries a higher flood risk, El Niño's impact is diminished by annual precipitation patterns in the analyzed areas, such as monsoonal and equatorial precipitation patterns. However, this does not imply that El Niño has no influence on the wet season in the analyzed area.

Nurdiati et al. (2022) and Sarvina (2023) have shown that El Niño can prolong the dry season, resulting in a shorter wet season during El Niño years. The extent of this impact varies by city, with El Niño potentially reducing the duration of the wet season by up to 28% (e.g., Manokwari). Despite having a shorter wet season, the annual precipitation in Manokwari during El Niño differs by only 2% compared to normal years (Sarvina, 2023). Conversely, a slightly longer wet season during La Niña can lead to significantly higher annual precipitation, such as a 7% extension of the wet season in Manokwari resulting in a 14% increase in annual precipitation. Consistent with the results of this research, La Niña tends to impact heavy precipitation in Papua, increasing the flood risk in the analyzed area. In contrast, the flood risk during El Niño does not decrease compared to normal years. This pattern is similar to the IOD's impact on flood risk in Papua, though it is less clear for both +IOD and -IOD.

While there is no specific research that explains the IOD's impact on precipitation characteristics in Papua, Indonesia, the influence of IOD can be estimated based on previous research and a logic similar to that applied to ENSO's impact. Okta et al. (2018) showed that during JJA, both -IOD and +IOD could increase precipitation in some regions of Papua while decreasing it in others, which is attributed to the different precipitation types in the region, as mentioned earlier. During SON, +IOD consistently decreases precipitation across all regions of Papua, whereas -IOD results in a wider range of impacts similar to those during JJA. Nevertheless, there is no significant correlation between precipitation and IOD during DJF and MAM (Okta et al., 2018). This is consistent with the results of this research, where IOD did not consistently impact precipitation distribution (**Fig. 7**). While +IOD

is positively correlated with the dry season and can extend its duration (Nurdiati et al., 2022), both +IOD and -IOD do not consistently affect higher precipitations. Both lead to an increase in the number of consecutive wet days, the number of heavy precipitations, and the number of heavy precipitations. The distributions of very wet day precipitations remain unchanged, while extreme wet day precipitations decrease, suggesting a reduced flood risk during both IOD phases.

The inconsistent impact of IOD on precipitation continues in the joint pattern analysis. In two examples of analyzed variables, all spatial patterns of West IOD and East IOD in **Fig. 8** and **Fig. 9** do not exhibit distinct patterns resembling either +IOD or -IOD phases. In all precipitation types depicted in the joint patterns, none display a clear spatial pattern of IOD's Sea Surface Temperature (SST), indicating the unclear impact of IOD on flood risk in Papua, Indonesia. Nonetheless, further research is required using different approaches and data to confirm the results of this research. This is particularly important because there is an increasing need for global assessments of flood risks in both current and future conditions to mitigate the impact of global warming (Winsemius et al., 2013).

5. CONCLUSIONS

The impact of ENSO and IOD on forest fires and flood risk in various regions of Papua, Indonesia varies due to the multi-precipitation patterns in the area. The consistent influence of the warm phase of both phenomena allows for the estimation of forest fire risk in the analyzed area. By combining three months of climate conditions, this research model can predict total monthly hotspots with more than 90% accuracy using elastic net regression. The accuracy of the estimation increases when ENSO and IOD indexes are integrated into the climate conditions, specifically in the dry spell. The integration concept is based on maximizing the positive correlation between climate conditions and forest fire indicators, as well as the positive correlation between ENSO and IOD indexes with the dry season, which leads to an increased forest fire risk in the analyzed area. With this level of accuracy, the model in this research can serve as a foundational model for robust prediction models to estimate monthly hotspots in Papua, Indonesia. However, it still needs further development to provide spatial and probabilistic information for hotspot estimation. Since forest fires in Papua, Indonesia primarily occurs in Merauke, future research can narrow down the analyzed area and use a combination of climatology stations and satellite data if feasible.

While the warm phase of ENSO and IOD consistently correlates positively with the dry season, both the cold phases of ENSO and IOD do not significantly impact heavy and extreme precipitation indicators in the analyzed area. Although La Niña tends to elongate the wet season duration in specific regions, the annual total precipitation during La Niña years is not significantly different from normal years. In an even more inconsistent manner, both +IOD and -IOD tend to increase the probability of higher heavy and extreme precipitation indicators in probability analysis. This inconsistent behavior is observed across all three precipitation patterns in Papua, including monsoonal, equatorial, and local precipitation patterns. However, the research addressing the impact of IOD on precipitation variability in Papua is limited, and most studies encompass wider areas rather than focusing on Papua, Indonesia. Therefore, further research is needed using different approaches, data sources, and perspectives to clarify the impact of IOD on flood risk in Papua. While ERA5 data accuracy has improved in recent years, different reanalysis precipitation data may perform differently depending on the analyzed area. As one of the wettest regions globally, the risk of flooding in Papua requires heightened attention since extreme weather events, whether related to ENSO/IOD or not, are predicted to occur more frequently as a consequence of global warming. This applies not only to La Niña years but also to El Niño years, which have a probability of higher precipitation similar to normal years.

REFERENCES

Al Jawarneh, A., Ismail, M. T., & Awajan, A. (2021) Elastic Net Regression and Empirical Mode Decomposition for Enhancing the Accuracy of the Model Selection. International Journal of Mathematical, Engineering and Management Sciences. 6. 564-583. 10.33889/IJMEMS.2021.6.2.034.

Ardiyani, E., Nurdiati, S., Sopaheluwakan, A., Septiawan, P., & Najib, M.K. (2023) Probabilistic Hotspot Prediction Model Based on Bayesian Inference Using Precipitation, Relative Dry Spells, ENSO and IOD. Atmosphere 2023, 14, 286. https:// doi.org/10.3390/atmos14020286

Arjasakusuma, S., Yamaguchi, Y., Hirano, Y., Zhou, X. (2018) ENSO- and Rainfall-Sensitive Vegetation Regions in Indonesia as Identified from Multi-Sensor Remote Sensing Data. ISPRS Int. J. Geo-Inf., 7, 103. https://doi.org/10.3390/ijgi703010

Björnsson, H., & Venegas, S. (1997) A manual for EOF and SVD analysis of climate data. Department of Atmospheric and Oceanic Sciences and Centre for Climate and Global Change Research, McGill University, Technical Report

Brenner, Norman M., Rader, Charles M. (1976). "A New Principle for Fast Fourier Transformation". IEEE Transactions on Acoustics, Speech, and Signal Processing. 24 (3): 264–266. doi:10.1109/TASSP.1976.1162805.

Breinl, K., Lun, D., Müller-Thomy, H., & Blöschl, G., (2021) Understanding the relationship between rainfall and flood probabilities through combined intensity-duration frequency analysis. J. Hydrol. 602, 126759. DOI: 10.1016/j.jhydrol.2021.126759.

Cane, M., & Zebiak, S. (1985) A Theory for El Niño and the Southern Oscillation. Science (New York, N.Y.). 228. 1085-7. 10.1126/science.228.4703.1085.

Ceccato, P., Jaya, I. N. S., Qian, J. H., Tippet, M. K., Robertson, A. W., & Someshwar, S. (2010) Early warning and response to fires in Kalimantan, Indonesia. IRI Technical Report: 10–14. Int Research Institute for Climate and Society, NY

Chatterjee, S. (2021) A New Coefficient of Correlation. Journal of the American Statistical Association, 116 (536), pp. 2009-2022

Choi, S. C., & Wette, R. (1969) Maximum Likelihood Estimation of the Parameters of the Gamma Distribution and Their Bias. Technometrics. 11 (4): 683–690. doi:10.1080/00401706.1969.10490731

Guerreiro, S. M., & Lajinha, T. (2007) Flood analysis with the standardized precipitation index (SPI). Revista da Faculdade de Ciência e Tecnologia. 4.

Haan, L., & Ferreira, A. (2007) Extreme value theory: an introduction. Springer.

Hannachi, A., Jolliffe, I.T. & Stephenson, D.B. (2007) Empirical orthogonal functions and related techniques in atmospheric science: A review. Int. J. Climatol., 27: 1119-1152. DOI: 10.1002/joc.1499

Hendon, H. H. (2003) Indonesian rainfall variability: impacts of ENSO and local airsea interaction. Journal of Climate. 16(11): 1775-1790.

Hendrawan, I.G., Asai, K., Triwahyuni, A., & Valentina, D. A. (2019) The interanual rainfall variability in Indonesia corresponding to El Niño Southern Oscillation and Indian Ocean Dipole. Acta Oceanol. Sin. 38, 57–66. DOI: 10.1007/s13131-019-1457-1

Hersbach, H., Bell, B., Berrisford, P., Hirahara, S., Horanyi, A., Sabater, J. M., Nicholas, J., Peubey, C., Biavati, G., Dee, D., & Flemming, J. (2020) The ERA5 Global Reanalysis. Quarterly Journal of the Royal Meteorological Society: DOI:10.1002/qj.3803. European Centre for Medium-Range Weather Forecasts, Reading, UK

Hidayat, R., Ando, K., Masumoto Y., & Luo, J. J. (2016) Interannual Variability of Rainfall over Indonesia: Impacts of ENSO and IOD and Their Predictability. IOP Conf. Ser.: Earth Environ. Sci. 31 012043. DOI: 10.1088/1755-1315/31/1/012043

Hui, Z., Junjun, Z,, Heng, X., & Xinkui, W. (2021) Singular value decomposition (SVD) based correlation analysis of climatic factors and extreme precipitation in Hunan Province, China, during 1960–2009. Journal of Water and Climate Change 12 (8): 3602–3616. doi: https://doi.org/10.2166/wcc.2021.398

Iskandar, I., Lestari, D.O., Saputra, A.D., Setiawan, R.Y., Wirasatriya, A., Susanto, R.D., Mardiansyah, W., Irfan, M., Rozirwan, Setiawan, J.D. & Kunarso. (2022) Extreme Positive Indian Ocean Dipole in 2019 and Its Impact on Indonesia. Sustainability 14, 15155. https://doi.org/10.3390/su142215155

Kurniadi, A., Weller, E., Min, S.-K., & Seong, M.-G. (2021) Independent ENSO and IOD impacts on rainfall extremes over Indonesia. Int J Climatol. 41: 3640– 3656. DOI: 10.1002/joc.7040

Lee, H.S. (2015) General Rainfall Patterns in Indonesia and the Potential Impacts of Local Seas on Rainfall Intensity. Water, 7, 1751-1768. DOI: 10.3390/w7041751

Li, J., Pollinger, F., & Paeth, H. (2020) Comparing the Lasso Predictor-Selection and Regression Method with Classical Approaches of Precipitation Bias Adjustment in Decadal Climate Predictions. Mon. Wea. Rev., 148, 4339–4351, https://doi.org/10.1175/MWR-D-19-0302.1.

McClean, F., Dawson, R., & Kilsby, C. (2021) Intercomparison of global reanalysis precipitation for flood risk modelling. DOI: 10.5194/hess-2021-153.

Navarra, A., & Simoncini, V. (2010) A Guide to Empirical Orthogonal Function for Climate Data Analysis: Springer. New York

Ngestu, R. N., & Hidayat, R., (2016) Influences of IOD and ENSO to Indonesian Rainfall Variability: Role of Atmosphere-ocean Interaction in the Indo-pacific Sector, Procedia Environmental Sciences 33, p. 196-203, DOI: 10.1016/j.proenv.2016.03.070

Nikonovas, T., Spessa, A., Doerr, S.H.; Clay, G.D., & Mezbahuddin, S. (2022) ProbFire: A probabilistic fire early warning system for Indonesia, Nat. Hazards Earth Syst. Sci. 22, 303–322.

Nurdiati, S., Sopaheluwakan, A., Julianto, M. T., Septiawan, P., & Rohimahastuti, F. (2021) Modelling and analysis impact of El Niño and IOD to land and forest fire using polynomial and generalized logistic function: cases study in South Sumatra and Kalimantan, Indonesia. Modeling Earth Systems and Environment, 8:3341–3356. DOI: 10.1007/s40808-021-01303-4

Nurdiati, S., Bukhari, F., Julianto, M.T. Sopaheluwakan, A., Aprilia, M., Fajar, I., Septiawan, P., &Najib, M. (2022) The impact of El Niño southern oscillation and Indian Ocean Dipole on the burned area in Indonesia. TAO 33, 16. DOI: 10.1007/s44195-022-00016-0

Okta, D. L., Sutriyono, E., Sabaruddin, S., & Iskandar, I. (2018) Respective Influences of Indian Ocean Dipole and El Niño-Southern Oscillation on Indonesian Precipitation. J. Math. Fund. Sci., Vol. 50, No. 3, 2018, 257-272

Olanrewaju, C. C., & Reddy, M. (2022) Assessment and prediction of flood hazards using standardized precipitation index—A case study of eThekwini metropolitan area. Journal of Flood Risk Management, 15(2), e12788. DOI: 10.1111/jfr3.12788

Pawitan, Hidayat. (1999) Enso Impact on Indonesia Seasonal Rainfall 1. Presented at the Asian Pacific FRIEND annd GAME Joint Workshop on ENSO, Floods and Droughts in the 1990's in Southeast Asia and the Pacific. Hanoi, Vietnam, 23-26 March 1999.

Prentice, M., & Hope, G. S. (2007) Climate of Papua and it's recent change: the ecology of Papua. Singapore. Periplus Edition: 177-195.

Rahmawati, F. A., Idung, R., & Fadli, S. (2011) Rainfall spatial and temporal variation analysis over Papua based on GSMAP during 1998-2006 and it‟s relation to the regional climate. Undergraduate Thesis, IPB University, Bogor (ID)

Randerson, J.T., G.R. van der Werf, L. Giglio, G.J. Collatz, and P.S. Kasibhatla. (2018) Global Fire Emissions Database, Version 4.1 (GFEDv4). ORNL DAAC, Oak Ridge, Tennessee, USA. https://doi.org/10.3334/ORNLDAAC/129

Rayner, N. A., Parker, D. E., Horton, E. B., Folland, C. K., Alexander, L. V., Rowell, D. P., Kent, E. C., & Kaplan, A. (2003) Global analyses of sea surface temperature, sea ice, and night marine air temperature since the late nineteenth century, J. Geophys. Res., Vol. 108, No. D14, 4407 10.1029/2002JD002670

Saji, N. H., Goswami, B. N., Vinayachandran, P. N., & Yamagata, T. (1999) A dipole mode in the tropical Indian ocean. Nature. 40(1):360–363. doi:10.1038/43854

Sarvina, Y. (2023) Enso and climate variability in Papua. IOP Conf. Ser.: Earth Environ. Sci. 1192 012041

Schroeder, W., Oliva, P., Giglio, L., & Csiszar, I. A. (2014) The new VIIRS 375m active fire detection data product: algorithm description and initial assessment. Remote Sensing of Environment, 143:85–96. doi:10.1016/j.rse.2013.12.008.

Syaufina, L., Nuruddin, A. A., Basharuddin, J., See, L. F., & Yusof, M. R. M. (2004) The effects of climatic variations on peat swamp forest condition and peat combustibility. Jurnal Manajemen Hutan Tropika. 10(1):1–14.

Tibshirani, R. (1996) Regression Shrinkage and Selection Via the Lasso. Journal of the Royal Statistical Society: Series B (Methodological), 58: 267-288. DOI: 10.1111/j.2517-6161.1996.tb02080.x

Towner, J., Cloke, H. L., Zsoter, E., Flamig, Z., Hoch, J. M., Bazo, J., Couglan, E. dP., & Stephens, E. M. (2019) Assessing the performance of global hydrological models for capturing peak river flows in the Amazon basin. Hydrology and Earth System Sciences, 23 (7), 3057–3080. doi: 10.5194/hess-23-3057-2019

Wiley E, & Hansen. (2014) Fourier Transform: Principles and Applications. New Jersey: J Wiley

Winsemius, H., Beek, L.P.H., Jongman, B., Ward, P., & Bouwman, A. (2013) A framework for global river flood risk assessments. Hydrol. Earth Syst. Sci. Discuss. 9. 9611-9659. DOI: 10.5194/hess-17-1871-2013.

Xiao, H.M., Lo, M.H. & Yu, J.Y. (2022) The increased frequency of combined El Niño and positive IOD events since 1965s and its impacts on maritime continent hydroclimates. Sci Rep 12, 7532. DOI: 10.1038/s41598-022-11663-1

Zou, H., & Hastie, T. (2005) Regularization and variable selection via the elastic net. Journal of the Royal Statistical Society: Series B (Statistical Methodology), 67: 301-320. DOIB: 10.1111/j.1467-9868.2005.00503.x